Experiments in Fluids 33 (2002) 135–142
DOI 10.1007/s00348-002-0459-y

Laser Doppler velocimetry measurement of turbulent bubbly channel flow

S. So, H. Morikita, S. Takagi, Y. Matsumoto

Abstract Measurements of the turbulence properties of gas–liquid bubbly flows with mono-dispersed 1-mm-diameter bubbles are reported for upward flow in a rectangular channel. Bubble size and liquid-phase velocity were measured using image-processing and laser Doppler velocimetry (LDV), respectively. A description is given of the special arrangements for two-dimensional LDV needed to obtain reliable bubbly flow data, in particular the configuration of the optical system, the distinction of signals from the bubbles and liquid phase. To create the mono-dispersed bubbles, a small amount of surfactant (3-pentanol of 20 ppm) was added to the flow. Whilst this caused a drastic change in bubble size distribution and flow field, it did not affect the turbulence properties of the single-phase flow. In this study, experiments with three different bulk Reynolds numbers (1,350, 4,100, 8,200) were conducted with void fractions less than 1.2%. In all three cases, there was a very high accumulation of bubbles near the wall with bubble slip at the wall. The mean velocity profile of the liquid phase was steeper near the wall owing to the driving force of buoyant bubbles, and the streamwise turbulent intensity in the vicinity of the wall was enhanced. Furthermore the mean velocity profiles of the liquid phase were flattened in the wide region around the channel center. This region was lifted up by the bubble sheet near the wall, giving it a plug-like flow structure. In addition, the turbulent fluctuation and Reynolds stress in the liquid phase are very much suppressed in this region. This strong preferential accumulation near the wall produces the dramatic change of the whole flow structure.

Received: 8 February 2002 / Accepted: 28 March 2002
Published online: 14 May 2002

S. So, S. Takagi (✉), Y. Matsumoto
Department of Mechanical Engineering, The University of Tokyo,
7-3-1 Hongo, Bunkyo-ku, Tokyo, 113-8656, Japan
E-mail: takagi@mech.t.u-tokyo.ac.jp
Tel.: +81-3-58416288
Fax: +81-3-58418542

H. Morikita
Morikita Shuppan Co. Ltd, 1-4-11, Fujimi Chiyoda-ku,
Tokyo 102-0071, Japan

The authors wish to express their gratitude to the helpful comments by Dr. Kazuyasu Sugiyama and Prof. Michael Reeks and the experimental support of Mr. Gota Kikugawa.

1 Introduction

Bubbly flows are observed in many industrial processes, such as the flows in chemical reactors, aeration tanks, and heat exchangers. Bubbly flows are also specifically utilized to reduce the friction drag of ships. Because of the wide application of these flows, many investigations on their turbulent structure have been carried out over the past two decades (for reviews, see Marie et al. 1997; Liu 1997). Some of them have provided us with some useful physical insights into the mechanisms involved. At the same time, considerable theoretical progress has been made. However, the structure of bubbly flows is generally very complicated, and it has thus proved very difficult to obtain experimentally reliable data on the detailed statistical properties of these flows.

The early studies on the measurement of bubbly flows were made by Serizawa et al. (1975) and Theofanous and Sullivan (1982), in which local measurements of liquid velocities and turbulent intensities in pipe flows were made using a hot-film anemometer and a laser-Doppler anemometer, respectively. Durst et al. (1986) measured the local fluid velocity around bubbles as well as the rising velocity, using a laser-Doppler anemometer. Following these studies, Wang et al. (1987), Lance and Bataille (1991), Serizawa et al. (1991) and Liu and Bankoff (1993a,1993b) experimentally provided information on: the local void fraction profile and its dependence on bubble size; the effect of initial bubble size on the bubbly flow structure and on the bubble-induced liquid turbulence. However, there is substantial disagreement amongst these experimental results, in spite of the fact that the experiments were performed under similar conditions. One of the reasons for this disagreement is considered to be the uncertainties in the mean and root mean square (rms) values of the bubble diameter. So, not surprisingly, there is no reliable information regarding the validity or otherwise of possible closure models for turbulent bubbly flow. As a first step towards better understanding and modeling of these flows, it is of paramount importance to carry out measurements under simple and well-defined conditions.

The objectives of the study reported here were to provide reliable statistical properties of turbulent bubbly flows under well-defined experimental conditions and to obtain information on the dominant features of the flow structure. To obtain well-defined experimental conditions, we generated small mono-dispersed bubbles about 1 mm in size by adding a small amount of 3-pentanol surfactant to the flow. The addition of this surfactant also has the

property of eliminating complicating factors such as bubble coalescence, unsteady vortex shedding behind the bubbles, and bubble deformation. The bubble size and the liquid-phase velocity were measured using image-processing and two-dimensional laser-Doppler velocimetry (2-D LDV), respectively. In this reported study, the flow fields were analyzed with the variation in void fraction and Reynolds number.

2 Experimental method

2.1 Experimental apparatus and conditions

The experimental apparatus and conditions are shown in Fig. 1 and Table 1, respectively. The experiments were conducted in a vertical circulating water tunnel, which was operated in the upward direction in the test section. The Reynolds numbers ($Re=U_b 2H/\nu$), based on the characteristic length of the channel width ($2H$=40 mm) and the bulk velocity of the liquid phase (U_b), were 1,350, 4,100, and 8,200. Here, the bulk velocity of the liquid phase can be estimated in two different ways. One method was the locally measured velocity profile by integrating the profiles across half the channel and dividing by half the channel width. The other method was from the globally measured liquid volumetric flux and dividing it by the cross-sectional area. There is a small difference of less than a few percentages between the values estimated using these two methods. This difference is caused by several factors, such as the effect of the side-wall, accuracy of the measured data, two-dimensionality at the test section etc. In the present study, we employed the method using the locally measured velocity profile, because the bulk velocity calculated from the liquid volumetric flux is not very reliable due to the effect of the side-wall.

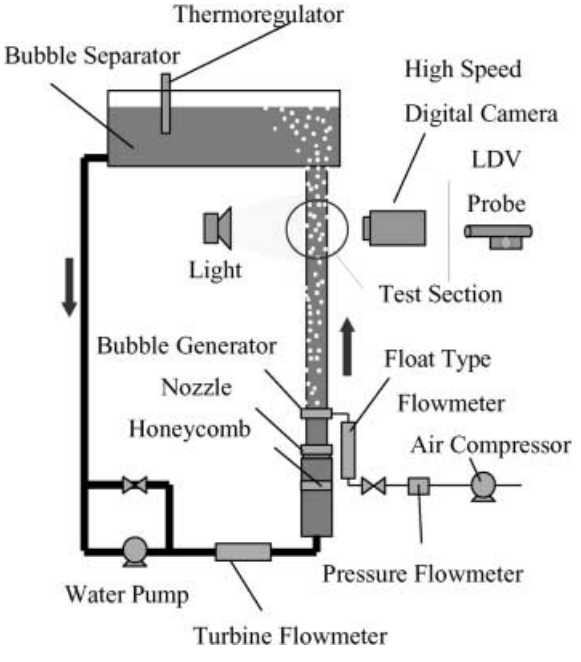

Fig. 1. Schematic figure of the experimental apparatus

The average gas volume fraction (f_g) varied from 0.3% to 1.2% and was estimated from the gas and liquid volumetric flux and the approximated bubble rising velocity using the following relation (Akagawa 1974):

$$f_g = \frac{1}{1 + (1/\beta - 1)S} \tag{1}$$

where S is the gas–liquid velocity ratio, and β is the volumetric flux ratio of the liquid and gas phase. S was based on the terminal velocity of an air bubble in water at 20°C, which is 0.12 m/s for a bubble diameter of 1.1 mm.

Throughout this paper, the coordinate x denotes the streamwise direction in the test section, and y denotes the perpendicular direction from the wall. The flow in the test section of the channel at 1,600 mm (x direction) above the bubble generator was expected to be fully developed (Dean 1978). The test section was 40 mm (y direction)×400 mm (z direction) with an aspect ratio of 10.

In order to avoid the ambiguity of experimental conditions such as bubble coalescence, the experiments were performed using spherical bubbles released uniformly in the cross section of the channel. To achieve this, the bubble generator, which created bubbles about 1 mm in diameter, was made up of a series of 474 stainless steel pipes of i.d. 0.07 mm and length 24 mm. These pipes were installed perpendicular to the flow to generate small bubbles from the shearing of the flow. The generator was installed above the inlet nozzle of the channel, which was located at x/H=80 downward from the test section.

The water flow rate was measured by a turbine flowmeter and the gas flow by a float type flowmeter. The average void fraction (f_g) was in the range of 0.3∼1.2%. The average bubble diameter and velocity of the bubbly flow were measured using a high-speed digital camera and 2-D LDV system, respectively.

2.2 Measuring system

In a preliminary experiment, bubble accumulation regions were observed near the wall, as suggested in Kashinsky et al. (1993), Liu and Bankoff (1993b) and Marie et al. (1997). This generated serious problems for x- and y-component LDV measurements, since the bubble accumulation eliminates the laser beams, distorts the

Table 1. Experimental conditions

Reynolds number Re (=$2U_bH/\nu$)	1,350		4,100		8,200	
Mean bulk velocity U_b (m/s)	0.029		0.092		0.176	
Reynolds number Re_τ (=$u_\tau H/\nu$)	–		147		260	
Wall Friction velocity u_τ (m/s)	–		0.00591		0–0.01043	
Average void fraction (f_g) (%)	0.6	1.2	0.3	0.6	0.3	0.6
Average diameter of bubbles (mm)	1.1					
Test section size (mm)	40($2H$)×400(W)×2,000(L)					

measuring volume and, consequently, decreases the data rate of the measurements. To overcome these problems, a commercial two-color fiber LDV system with a modified transmitting unit was used.

Figure 2 shows the optical arrangement of the LDV system, which consisted of a commercial instrument (FLV 8835, Kanomax, Osaka) and additional optical components. x and y velocities were measured by beams of 514.5 nm (green) and 488.0 nm (blue) wavelengths, respectively. Scattered light was collected by the same lens as the transmitting optics for the green beams and was detected by two photomultipliers for each color. The whole transmitting and receiving units were mounted on a single optical bench with a traversing system.

The optical plane of the green beams was inclined 3° relative to the wall to avoid elimination by high concentrations of bubbles. The measuring volume of the blue beams was focused at the same position as the green beams, through a transparent rectangular "tank" filled with water (see Fig. 2). This ensured that the measuring volumes of the green and blue beams were coincident at all measuring points in the test section. As a consequence, simultaneous two-component velocity measurement was successfully achieved with the required accuracy, spatial resolution and data rate. Optical parameters are summarized in Table 2.

Output signals from the photodetectors were amplified and subsequently digitized by A/D converter (Gage CSLITE, Montreal, Canada). Velocities were calculated by fast Fourier transform-based software with the validation criteria suggested in Kobashi et al. (1990). The maximum data rate was approximately 1,000/s.

Spherical mono-dispersed polystyrene particles of 8 μm average diameter (density ρ=1,070 kg/m^3) were used as seeding particles. The terminal velocity and the relaxation time of particles in water were 3×10^{-6} m/s and 3×10^{-7} s, respectively. In the present experiment, the Kolmogorov length and time scale in the test section were estimated to be of the order of 100 μm and 10 ms,

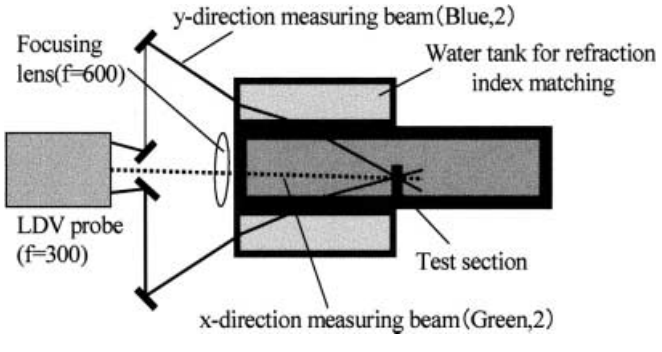

Fig. 2. Configuration of the LDV probe and the test section

Table 2. Optical parameters of LDV system

Laser wavelength (nm)	514.5 (green)	488.0 (blue)
Laser power (mW)	10	7.5
Size of the measuring volume at $1/e^2$ ($\Delta x\times\Delta y\times\Delta z$) (mm^3)	0.16×0.16×2.3	0.24×0.22×0.54
Fringe spacing (μm)	5.155	0.595

respectively. Therefore, seeding particles used in the present study have a sufficiently high response to follow the liquid-phase motion precisely.

In these particular bubbly flows, the liquid velocity was obtained from the signal of the light scattered from the seeding particles. However, distinction of the signal for seeding particles from all the signal of the bubbly flows was not easy to obtain because dispersed bubbles also act as a source of scattering of the laser light. In the present study, the following procedures were used to distinguish the signals.

1. Control the trigger level of the signal intensity, using the difference between Doppler signals from seeding particles and bubbles. This was required because the signals from the bubble were much larger than those of the seeding particles due to the larger size of bubbles.
2. Ensure that the data rate of the seeding particles overwhelms that of bubbles by increasing the number density of the seeding particles.
3. Remove the velocity data of the bubbles from those of the whole flow, using the relative velocity between the liquid phase and the bubbles.

In procedure (3), we need a large relative velocity between the liquid phase and the bubbles. This relative velocity is used to divide the LDV signals into two classes, one from the liquid phase and the other from the bubbles. Except in the vicinity of the wall, the signals are well classified and data noise due to the bubble motion can be distinguished from that of bubbly flows. However, the velocity signals in the vicinity of the wall are not easy to divide into these two different classes. This is because the relative velocity between liquid and gas phases becomes small in this region. Therefore, the classification of the signals was carried out for the data except those in the vicinity of the wall.

Following Yanta and Smith (1978), the sampling number was chosen as 3,000, which gave relative errors of mean and standard deviation of 1.8% and 2.5%, respectively. The origin of the coordinates was determined from the scattered light from the wall. Then, after the measurement of velocity profile, the position was confirmed by the coincidence of the measured velocity profile and that obtained from the log-law of the wall. The uncertainty of the position was ±50 μm.

3
Experimental results and discussion

3.1
Distribution of bubble diameters

The average diameter of bubbles injected from the bubble generator was measured by means of a high-speed digital camera (MEMRECAM ci V-140-J, NAC Image Technology, Tokyo, Japan). Figure 3 shows typical results of the distribution of bubble diameters. The results correspond to the case of Re=1,350 and 4,100 at a void fraction of 0.6%. "Without Pentanol" in Fig. 3 refers to the results for water flow without the addition of 3-pentanol surfactant. In this case, the average diameter was about 1.85 mm and the standard deviation of the distribution about 0.50 mm,

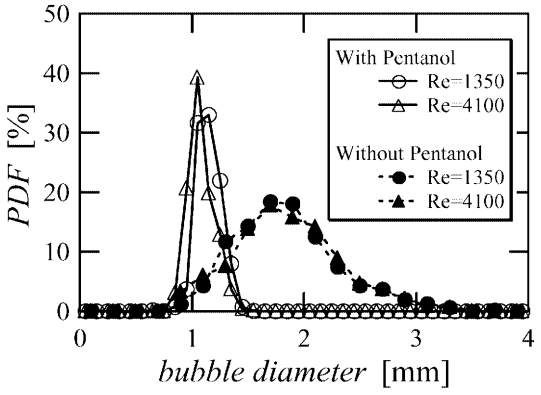

Fig. 3. Bubble size distributions of void fraction 0.6%

which was not good enough for our "mono-dispersed" requirements. To investigate the reason for the large standard deviation of bubble size, we observed the size history of a bubble released from the needle. It was found that bubbles coalesce several times before they reach the test section. Since it is known that the coalescence of bubbles is prevented by the addition of a small amount of surfactant, 20 ppm of 3-pentanol ($C_5H_{11}OH$) was injected into the flow. It was directly injected in circulating water flow by a syringe with accurate notch marks on a scale. 3-Pentanol is soluble in water, and it takes about several minutes to be well mixed in the circulating channel, which is recognized from the observation of bubble behavior. Then, we measured the velocity signals of the LDV at a certain measuring point. It is confirmed that the signal is sufficiently stabilized in about 30 min after the injection of 3-pentanol. In the present experiment, the measurement of the velocity is started at least 1 h after the injection. Figure 3 also shows the results of adding this surfactant. In these cases, the average diameter based on the projected area was 1.11 mm, with a standard deviation of 0.11 mm and was thus much more compatible with our "mono-dispersed" requirements.

Figure 4 shows photographs of the bubbles in the test section at a Reynolds number of 8,200 and a void fraction (f_g) of 0.60%. It is clearly observed that the bubble size and the size distribution were drastically changed by the addition of 3-pentanol. This change also produced a dramatic change in the whole bubbly flow structure.

In the water flow without the surfactant, the larger bubbles rose with a zigzag leaping motion against the perpendicular wall and were distributed throughout the cross section of the channel. It was also observed that this kind of leaping motion of a bubble enhances the mixing of the fluid and seemed to produce the large fluctuations in the flow. Furthermore, once the small amount of 3-pentanol was added, the whole aspect of the flow field was changed. Bubbles started accumulating near the wall and sliding along it. It is also interesting to note that the accumulated bubbles near the wall formed horizontal bubble clusters 20–40 mm in length, which rose and oscillated like moving waves.

3.2
Single-phase flow

To investigate the effect of added 3-pentanol on the fully developed turbulent channel flow, the streamwise mean velocity and turbulent fluctuations were measured for the single-phase flow by the LDV system. The results are shown in Fig. 5. Figure 5a shows the mean velocity profiles of single-phase flow at Re_τ =147, which corresponds to Re=4,100, for the water flow with/without 20 ppm of 3-pentanol. It is evident that the difference between the two cases is very small and is not clearly recognized in the figure. Figure 5a also shows the comparison of the results with the law of the wall and that of direct numerical simulation (DNS) at nearly the same Reynolds number based on the wall friction velocity, which is Re_τ=150 (Kasagi et al. 1992). Regardless of the addition of 3-pentanol, the present results show an excellent agreement with the law of the wall and the DNS result. The turbulent fluctuations normalized by the wall friction velocity are shown in Fig. 5b, which are also in good agreement with DNS result in both x and y directions, regardless of the addition of 3-pentanol. Thus, the comparison with DNS data shown in Fig. 5a, b confirms that the measuring system was reliable. And through the comparison of the results with and without 3-pentanol, it is concluded that the effect of added 3-pentanol to the single turbulence flow was negligibly small and the drastic changes of the flow field by the addition of 3-pentanol were caused only in the presence of bubbles.

3.3
Air–water bubbly flow

The experimental results of the bubbly flow with added 3-pentanol (20 ppm) are shown in Fig. 6, 7, 8, 9, and 10. Figure 6 shows the mean velocity profiles of the liquid

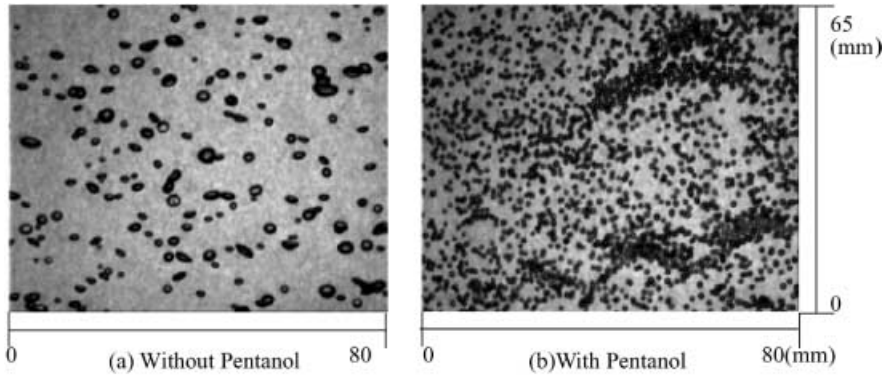

Fig. 4a, b. Photos of the bubbles in the test section at Re=8,200 and f_g=0.60%: **a** without pentanol; **b** with pentanol

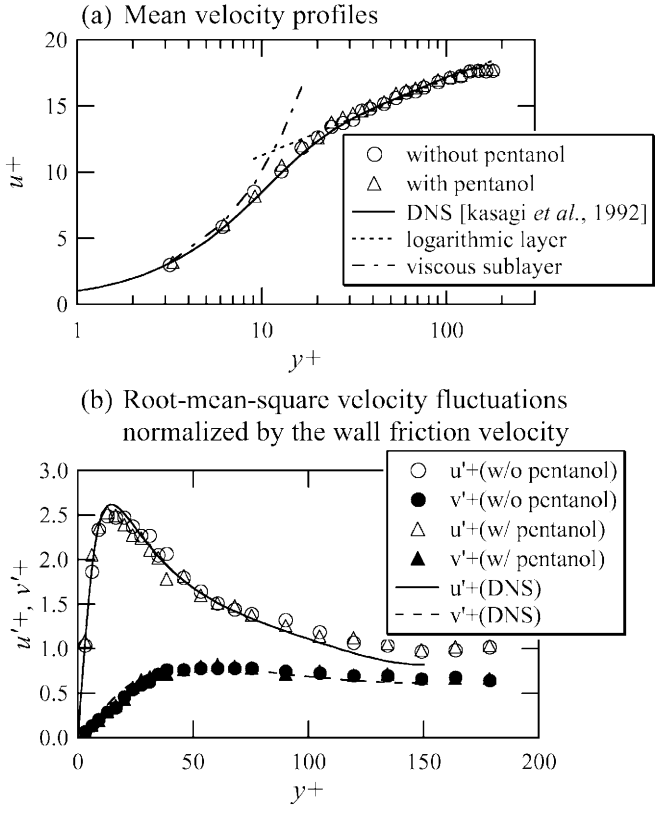

Fig. 5a, b. Comparisons between the experiment results with/without 3-pentanol (Re_τ=147) and the DNS results (Re_τ=150) (single-phase flow): **a** mean velocity profiles; **b** rms velocity fluctuations normalized by the wall friction velocity

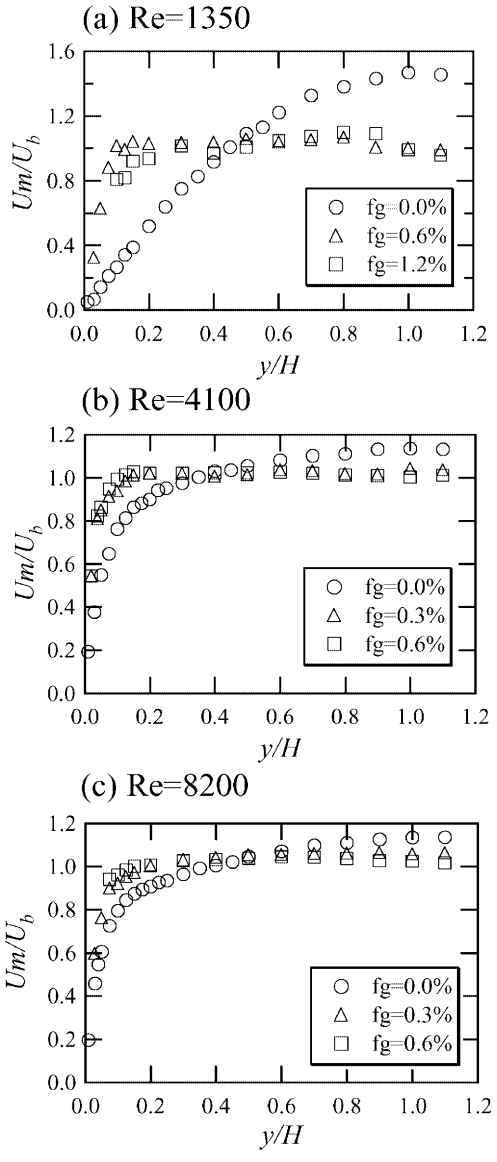

Fig. 6a–c. Mean velocity profiles of the liquid-phase flow: **a** *Re*=1,350; **b** *Re*=4,100; **c** *Re*=8,200

phase normalized by the bulk velocity versus the distance from the wall. The experimental conditions are shown in Table 1. The velocity profile at *Re*=1,350 without bubbles (f_g=0.0%) is shown in Fig. 6a. For *Re*=1,350, the flow was expected to be the laminar flow, and this is consistent with the observed parabolic profile. This parabolic profile was drastically changed after the injection of bubbles. After the injection, the mean velocity profiles of the liquid phase became turbulent-like profiles, that is, there was a large velocity gradient near wall with a flat profile in the middle of channel. The velocity gradient near the wall became steeper with the increase in void fraction. This velocity profile was brought about by the rising motion of bubbles accumulated near the wall. Figure 6b, c corresponds to the mean velocity profile of the liquid phase at *Re*=4,100 and 8,200, respectively. Although the velocity profile without bubbles (f_g=0.0%) was that of a turbulent flow and were quite different from the results for *Re*=1,350, a similar tendency was observed after the injection of bubbles. That is, the velocity gradient near the wall became steeper and that in the center of the channel flattened with the increase in void fraction.

Figure 7 shows the streamwise turbulent fluctuations normalized by the mean bulk velocity versus the distance from the wall. Since the flow field without bubbles (f_g=0.0%) in Fig. 7a corresponded to the single-phase laminar flow, it has few fluctuations. With bubbles, however, the fluctuations are produced by the motion of rising bubbles and by the pseudo-turbulence effect of bubbly flows. These fluctuations in the liquid phase are clearly observed in Fig. 7a for f_g=0.6% and 1.2%. It is noted that the fluctuations given by the bubble motion were significantly different from those given in the single-phase turbulence. Figure 7b, c corresponds to the cases where the flow field without bubbles was turbulent.

Under these conditions, the turbulent fluctuations in the vicinity of the wall (where there is bubble accumulation) were enhanced by the pseudo-turbulence effect induced by the motion of bubbles. From the single-phase data in Fig. 6, it is shown that the liquid velocity gradient near the wall increases with increasing Reynolds number. Consequently, as shown in Fig. 7, the peak position of the turbulent fluctuations becomes closer to the wall with increase in Reynolds number. In contrast, in the bubbly flows, its position corresponds to the location of the bubble accumulation region.

Figures 8 and 9 show the mean velocity profiles and dimensional turbulent fluctuation profiles, respectively.

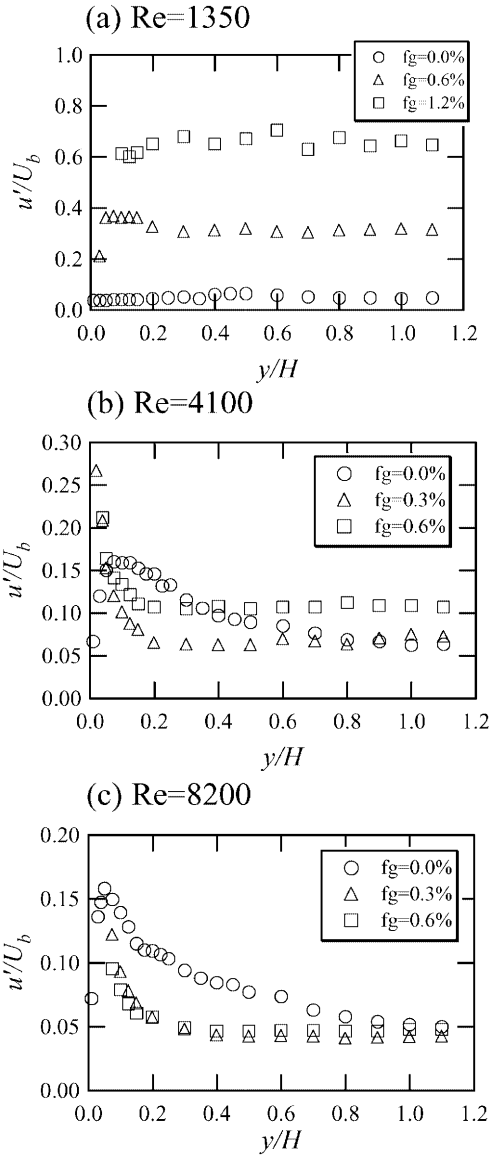

Fig. 7a–c. Rms velocity fluctuations of the liquid-phase flow: **a** *Re*=1,350; **b** *Re*=4,100; **c** ***Re***=8,200

The experimental conditions shown in the figures correspond to the same void fraction but with a different Reynolds number. Regardless of the flow state (laminar or turbulent) as single-phase flows, the velocity profiles of the corresponding bubbly flows are very similar to each other and have little dependence on the Reynolds number. It is also interesting to note that the dimensional fluctuations in Fig. 9 quantitatively coincide over the channel width except the near wall. This result gives some very important information on the structure of bubbly flow. It suggests that the fluctuations in this region are not related to the turbulence characteristics and are produced by the bubble motions in the flow which have small fluctuations.

Figure 10 shows the Reynolds stress profile of the liquid phase. As mentioned above, in the case of a bubbly flow, the fluctuations over most of the channel width were mainly supplied by the rising motions of bubbles. Although most of bubbles accumulated near the wall, a small number of bubbles rose up in this region and created small

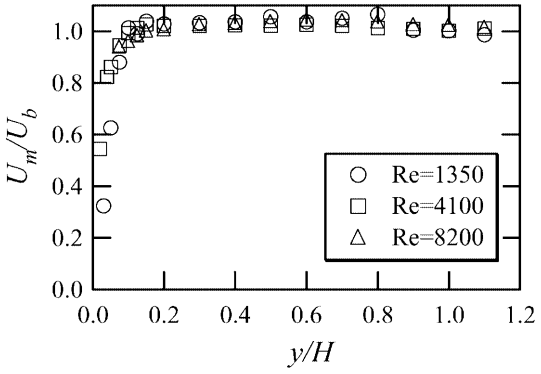

Fig. 8. Mean velocity profiles under different Reynolds numbers (void fraction of 0.6%)

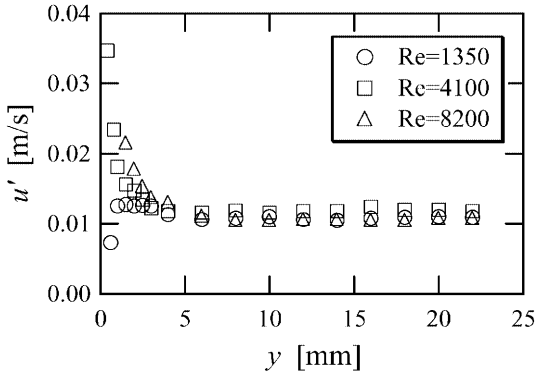

Fig. 9. Rms velocity fluctuations with the variations in Reynolds number (void fraction of 0.6%)

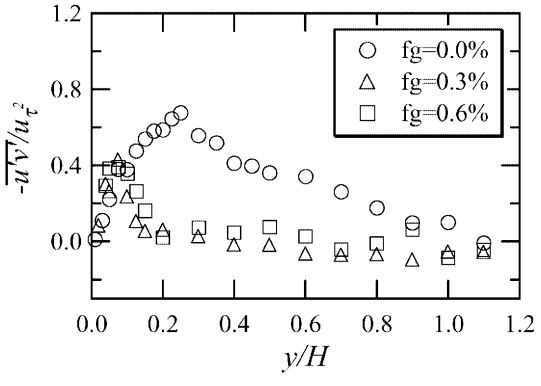

Fig. 10. Reynolds stress of liquid phase normalized by the wall friction velocity (*Re*=4,100)

fluctuations. Since these fluctuations are not a source of Reynolds stress, Fig. 10 clearly shows that the Reynolds stress in this region is much smaller than that of single-phase flows. From the turbulence theory of single-phase flow, the sum of viscous stress and Reynolds stress must be constant across the channel. Since this flow has a strong buoyancy effect near the wall, where the many bubbles accumulate, this relation is not necessarily satisfied and actually the flow itself behaves more like a plug flow with a small Reynolds stress.

The present phenomena can be summarized as follows. Regardless of whether the single-phase flow is laminar or

turbulent, bubbles start accumulating near the wall due to the lateral lift force caused by the mean shear around each bubble. If the bubbles are nearly spherical (as was the case here) and rise up in the upward flow, there are, at least, two ways of causing the lateral migration of bubbles. One way is from the action of the lift force due to the presence of the mean shear and the other is from the action of the lateral pressure gradient from the gradient in the Reynolds stresses of the bubbly flow normal to the wall. These two forces are roughly estimated using the single-phase data and using the well-known lift force model of Auton (1987). It was found in our experiments that the lift force is more than 100 times greater than the force due to the lateral pressure gradient, from which we conclude that the lift force was the dominant force causing the migration of the bubbles towards the wall. Due to this lateral force, bubbles form a high void fraction region near the wall and slide up it. At this stage, most of the bubbles are sliding up at the same distance from the wall. The nature of the force balance at this distance is not clear. One possible explanation is that this equilibrium distance arises from a force balance between the lift force toward the wall and the pressure gradient away from the wall. As mentioned above, in most of the channel width, the lift force exceeds the force due to the lateral pressure gradient of liquid phase and forces the bubbles to accumulate in the vicinity of the wall. But the repulsive force from the wall due to the pressure gradient increases as the wall is approached, and it is possible that both forces balance in the vicinity of the wall. Another possibility is that the complicated interaction between bubbles, wall and shear creates this equilibrium distance. It is clear that more investigation is required to establish the precise nature of this mechanism.

Once the bubble accumulation has occurred, bubbles at this position form clusters and behave like a sheet of bubbles. This bubble sheet pulls up the surrounding liquid by its buoyancy. Then, the mean velocity profile of the liquid phase becomes steeper near the wall due to this driving force and the streamwise turbulent intensity in the vicinity of the wall is enhanced. Furthermore, the mean velocity profiles of the liquid phase are flattened in the wide region of the channel center, whilst the turbulent intensity becomes much lower than that of single-phase flow in the intermediate region ($0.1 \leq y/H \leq 0.6$). This is because the large driving force from buoyant bubbles drastically changes the flow structure in the intermediate region. Most of region (except in the vicinity of the wall) is suspended by the near-wall bubble sheet, and a plug-like flow structure occurs. The turbulent fluctuations and Reynolds stress in the liquid are very much suppressed in this region. Thus, two regions separated by the bubble sheet have different origins for velocity fluctuations. In the narrow region between the wall and the bubble sheet, the fluctuations are produced mainly by high shear rate turbulence. In the other regions, fluctuations are caused by the motion of bubbles rising in plug-like flow with much less fluctuation.

Several researchers, i.e. Wang et al. (1987), Lance and Bataille (1991), Liu and Bankoff (1993a) and Marie et al. (1997) etc., reported that the liquid fluctuations are reduced under the high liquid velocity conditions. But the mechanism is not yet well understood. The present results show the same tendency. Since the bubbles reported here are well controlled as mono-dispersed spherical bubbles, it is possible to evaluate several factors separately and then to suggest the detailed mechanism for this phenomenon. That is, the plug-like flow structure with small fluctuations was expected from the data obtained. And the result of Fig. 9 clearly shows that the fluctuations in the center region are produced not by turbulence but by the motion of bubbles.

It is known that the turbulence in the bubbly flow compared with that in the single-phase flow is enhanced at high void fraction, while it is suppressed at low void fraction. The maximum threshold of the void fraction to suppress the turbulence in the present study is higher than that in the previous experiments of Serizawa et al. (1975), Wang et al. (1987) and Liu and Bankoff (1993a). This might be explained by the fact that the bubble size in the present study is smaller than that in the previous experiments and that the large superficial area of the present small bubbles promotes the dissipation of the turbulent kinetic energy. But the following explanation is also possible, namely that the present bubbles are much more affected by the lift force toward the wall. Since the direction and amplitude of the lateral lift force is sensitive to the bubble size, it is possible that the reason for the suppressed fluctuations is the modification of the global flow structure caused by the accumulation of bubbles in the vicinity of the wall.

4
Summary and conclusions

An investigation of the channel flow with dispersed spherical bubbles was conducted using image processing and the 2-D LDV systems. By adding a small amount of 3-pentanol as surfactant, mono-dispersed small spherical bubbles of 1 mm diameter were uniformly generated across the channel. The addition of the surfactant drastically changed not only the bubble size and the size distribution but also the macroscopic flow structures. A 2-D LDV measurement system was carefully set up to reliably measure the statistical properties of turbulent bubbly flows. Special arrangements were made for the laser beam path to avoid interruption by the bubbles and for the signal processing to select the light from seeding particles.

The measured data for single-phase turbulence showed very good agreement with the well-known DNS data. Furthermore, the addition of 3-pentanol had no effect on the statistical properties of single-phase flows. Hence, we used this system to investigate the turbulent bubbly flows.

Experiments with three different conditions of bulk Reynolds numbers (1,350, 4,100, 8,200) were conducted with a void fraction of less than 1.2%. Under these conditions, the bubbles accumulated near the wall with very high concentrations and slid up along the wall regardless of the Reynolds number. The accumulated bubbles near the wall formed clusters of about 20–40 mm in size which had a thin crescent-like shape as shown in Fig. 4. These clusters appeared in many places near the wall and behaved like a sheet sliding up near the wall. This bubble sheet lifts up the surrounding liquid owing to buoyancy.

Then, the mean velocity profile of the liquid phase became steeper near the wall owing to this driving force, and the streamwise turbulent intensity in the vicinity of the wall was enhanced. Furthermore, the mean velocity profiles of the liquid phase were flattened in the wide region of the channel center. This region was sustained by the bubble sheet near the wall, and a plug-like flow structure developed. The turbulent fluctuation and Reynolds stress in the liquid phase were very much suppressed in this region. It was noted that the main contribution to the fluctuation observed in this region was due to the rising motion of bubbles, where the local void fraction in this region was much lower than that in the near-wall region.

Finally it is emphasized that nearly spherical 1-mm bubbles in upward flow had a very strong preferential accumulation near the wall which resulted in a dramatic change in the whole flow structure.

References

Akagawa K (1974) Gas–liquid two-phase flow. Corona Publishing, Tokyo, pp 36–37 (in Japanese)

Auton TR (1987) The lift force on a spherical body in a rotational flow. J Fluid Mech 183:199–218

Dean RB (1978) Reynolds number dependence of skin friction and other bulk flow variables in two–dimensional rectangular duct flow. J Fluids Eng 100:215–223

Durst F, Shönung B, Selanger K, Winter M (1986) Bubble-driven liquid flows. J Fluid Mech 170:53–82

Kasagi N, Tomita Y, Kuroda A (1992) Direct numerical simulation of passive scalar field in a two dimensional turbulent channel flow. J Heat Transfer 114:598–606 (DNS data are supplied from the Kasagi Lab DNS database: http://www.thtlab.t.u-tokyo.ac.jp/DNS/dns_database.html)

Kashinsky ON, Timkin LS, Cartellier A (1993) Experimental study of "laminar" bubbly flows in a vertical pipe. Exp Fluids 14:308–314

Kobashi K, Hishida K, Maeda M (1990) Measurement of fuel injector spray flow of I.C. engine by FFT based phase Doppler anemometer. Application of laser technique to fluid mechanics. Springer, Berlin Heidelberg New York, pp 268–287

Lance M, Bataille J (1991) Turbulence in the liquid phase of a uniform bubbly air–water flow. J Fluid Mech 222:95–118

Liu TJ (1997) Investigation of the wall shear stress in vertical bubbly flow under different bubble size conditions. Int J Multiphase Flow 23:1085–1109

Liu TJ, Bankoff SG (1993a) Structure of air–water bubbly flow in a vertical pipe–I. liquid mean velocity and turbulence measurements. Int J Heat Mass Transfer 36:1049–1060

Liu TJ, Bankoff SG (1993b) Structure of air–water bubbly flow in a vertical pipe–II. Void fraction, bubble velocity and bubble size distribution. Int J Heat Mass Transfer 36:1061–1072

Marie JL, Moursali E, Tran-Cong S (1997) Similarity law and turbulence intensity profiles in a bubbly boundary layer at low void fractions. Int J Multiphase Flow 23:227–247

Serizawa A, Kataoka I, Michiyoshi I (1975) Turbulence structure of air–water bubbly flow–II. local properties. Int J Multiphase Flow 2:235–246

Serizawa A, Kataoka I, Gofuku A, Takahashi O, Kawara Z (1991) Effect of initial bubble size on bubbly flow structure. In: Proceedings of the International Conference on Multiphase Flow, Tsukuba, Japan, pp 547–550

Theofanous TG, Sullivan J (1982) Turbulence in two-phase dispersed flows. J Fluid Mech 116:343–362

Wang SK, Lee SJ, Jones OC Jr, Lathey RT Jr (1987) 3-D turbulence structure and phase distribution measurements in bubbly two-phase flows. Int J Multiphase Flow 13:327–343

Yanta WJ, Smith RA (1978) Measurements of turbulence-transport properties with a laser Doppler velocimeter. AIAA 11th Aerospace Science Meeting, AIAA Paper 71–287